Virtual Passive-Joint Space Based Time-Optimal Trajectory Planning for a 4-DOF Parallel Manipulator

Jie Zhao, Guilin Yang, *Member, IEEE*, Haoyu Shi, Silu Chen, *Member, IEEE*, Chin-Yin Chen, *Member, IEEE*, and Chi Zhang, *Senior Member, IEEE*

***Abstract*—The 4-DOF (3T1R) 4PPa-2PaR parallel manipulator is developed for high-speed pick-and-place operations. However, conventional trajectory planning methods in either active-joint space or Cartesian space have some shortcomings due to its high nonlinear kinematics. Owing to its unique four-to-two leg structure, the middle link that connects to the two proximal parallelogram four-bar linkages in each side only generates 2-DOF translational motions in a vertical plane. By treating each of the middle link as a 2-DOF virtual passive joint, a new trajectory planning method in the 4-DOF virtual passive-joint space is proposed, which not only simplifies the kinematic analysis, but also decreases the kinematics nonlinearity. By introducing the virtual passive joints, both displacement and velocity analyses are readily investigated. The Lagrangian method is employed to formulate the closed-form dynamic model. The quintic B-spline is utilized to generate trajectories in the virtual passive-joint space, while the Genetic Algorithm is implemented to search for the time-optimal trajectory. The simulation results show that the motion time planned in the virtual passive-joint space is decreased by 2.8% and 8.1% compared with the active-joint space method and Cartesian space method respectively. The average and peak jerks of the moving platform are decreased by 14.6% and 37.6% compared with the active-joint space method.**

***Index Terms*—Parallel manipulator, trajectory planning, virtual passive joints, quintic B-spline, minimum time optimization.**

I. Introduction

TRAJECTORY planning of *Parallel Manipulators* (PMs) for high-speed pick-and-place operations, has a wide range of industrial applications, such as food sorting, parts assembling and material handing. In general, a desired trajectory should possess the attributes of short execution time, low energy consumption, continuous acceleration, and low jerk for both the active joints and the moving platform. Over the last few decades, significant research efforts have been made to generate the desired trajectories for high-speed pick-and-place operations. Nevertheless, most of the trajectory planning approaches can be classified into two categories: the active-joint space method and the Cartesian space method.

The active-joint space method is to obtain the displacements of active joints through inverse kinematics given the via points of the moving platform. For the high-speed pick-and-place operation, the most popular one describing the general geometric path in Cartesian space is based on five via points, i.e., initial point, lift-off point, middle point, set-down point, and final point, which depicts the motion profile clearly with low computation burdens [1]. To achieve continuous velocities, accelerations, and jerks of the trajectory, interpolation functions such as polynomials [2], [3], spline curves [4], [5], [6], and other blending functions [7], [8] are utilized directly in the active-joint space. The active-joint space method has a few advantages such as smooth trajectory with low jerks, small average and peak driving forces of the active joints, and low computation burden. However, its performances are usually limited by the high nonlinear kinematics of the PM, which may not only increase the jerk values of the moving platform, but also decrease the path accuracy in Cartesian space.

For the Cartesian space method, the conventional path is formed by connecting the horizontal and vertical segments with arcs, which increases the computation burden due to large numbers of parameters and constraint conditions. To depict the path shape directly in Cartesian space, the path equations, such as semi-elliptic [9], Lame curve [10], and Pythagorean Hodograph curve [11], are employed, but they are hard to achieve high order trajectory continuity. Currently, the trajectory planning method based on quintic B-spline model is used widely in Cartesian space [12], [13], [14]. This approach decreases the computation burden due to fewer via points in geometric path, and achieves jerk continuity of trajectories. Although the Cartesian space method can generate smooth trajectory and accurate geometric path of the moving platform, the method is limited due to the kinematic nonlinearity, which results in the decreased trajectory performances of the active joints, and its computation time is also increased due to the existence of multiple inverse kinematics solutions.

Manuscript received 2 February 2023; accepted 1 June 2023. Date of publication 3 July 2023; date of current version 11 July 2023. This letter was recommended for publication by Associate Editor H. Kong and Editor L. Pallottino upon evaluation of the reviewers' comments. This work was supported by the Zhejiang Provincial Key Research and Development Plan under Grant 2021C01069. *(Corresponding author: Guilin Yang.)*

Jie Zhao and Guilin Yang are with the Zhejiang Key Laboratory of Robotics and Intelligent Manufacturing Equipment Technology, Ningbo Institute of Materials Technology and Engineering, Chinese Academy of Sciences, Ningbo 315201, China, and also with the University of Chinese Academy of Sciences, Beijing 100049, China (e-mail: zhaojie@nimte.ac.cn; glyang@nimte.ac.cn).

Silu Chen, Chin-Yin Chen, and Chi Zhang are with the Zhejiang Key Laboratory of Robotics and Intelligent Manufacturing Equipment Technology, Ningbo Institute of Materials Technology and Engineering, Chinese Academy of Sciences, Ningbo 315201, China (e-mail: chensilu@nimte.ac.cn; chenchinyin@nimte.ac.cn; zhangchi@nimte.ac.cn).

Haoyu Shi is with the Zhejiang Key Laboratory of Robotics and Intelligent Manufacturing Equipment Technology, Ningbo Institute of Materials Technology and Engineering, Chinese Academy of Sciences, Ningbo 315201, China, and also with the University of Nottingham Ningbo, Ningbo 315201, China (e-mail: shihaoyu@nimte.ac.cn).

Digital Object Identifier 10.1109/LRA.2023.3291896

To overcome such limitations, three major types of approaches have been proposed. The first type improves trajectory performances by using a hybrid or modified interpolation algorithm [13], [15]. However, the approach introduces a few parameters and constrains, which increases the computation burden. The second type employs comprehensive objective functions in trajectory optimization models, such as minimum sum of acceleration and jerk with weight coefficients [1], [14], jerk norm and standard deviation [11], and the square of the sum of acceleration and time [16]. Although the smoothness of trajectories is improved, the optimization model is complicated and the weight coefficients are hard to be determined. The third type reduces the mathematical complexity based on the kinematic features of the PM such as isotropic [17], which possesses the constant and diagonal Jacobian matrices so as to decrease the kinematic nonlinearity, but it is limited by the configuration of PMs.

A PM normally has multiple passive joints. In general, the kinematic relationships between the passive joints and both of the active-joint and the moving platform can be readily obtained, and for which their kinematics nonlinearities are significantly reduced. Taking the advantage offered by passive joints, a simplified singularity analysis method based on passive-joint velocities has been successfully developed [18]. As such, it could be also effective to plan the trajectory in virtual passive-joint space so as to obtain desired performances in both of the active-joint space and Cartesian space.

The novelties and contributions of this letter are presented as follows:

1) Owing to the unique kinematics characteristics of the 4PPa-2PaR PM, it is realized that the middle link that connects two proximal parallelogram four-bar linkages to one distal parallelogram four-bar linkages in each of the two branches always generates the 2-DOF translational motions in a fixed vertical plane. By treating each of the middle links as a 2-DOF virtual passive joint, simple kinematic relationships from the virtual passive joints to both the active joints and the moving platform are obtained, which makes the nonlinearity of the resultant kinematic models reduced.
2) A new time-optimal trajectory planning method in the 4-DOF virtual passive-joint space is proposed for the 4PPa-2PaR PM. which generates the fastest trajectory compared with the trajectory planning methods in both the active-joint space and Cartesian space under the same performance constraints. The simulation results show that the trajectory time planned in passive-joint space is decreased by 2.8% and 8.1% compared with the active-joint space method and Cartesian space method, respectively.

The rest of this letter is organized as follows. In Section II, the displacement and velocity kinematics from the virtual passive joints to both active joints and the moving platform are investigated, while the dynamic model is formulated by the Lagrangian method. Section III establishes the trajectory model by quintic B-splines. In Section IV, a trajectory optimization algorithm based on Genetic Algorithm for achieving minimum trajectory time is developed. A simulation example is given in Section V, and the effectiveness of the virtual passive-joint space method is validated. Section VI concludes this letter.

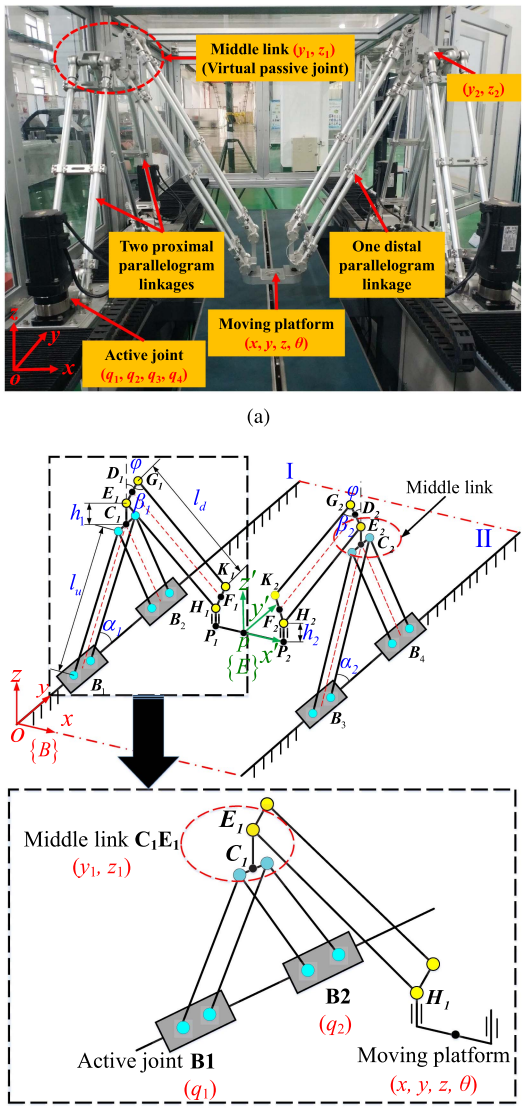

Fig. 1. Configuration of the 4PPa-2PaR PM: (a) Prototype of the 4PPa-2PaR PM. (b) Kinematic diagram of the 4PPa-2PaR PM.

II. Kinematic and Dynamic Modeling

A. Description of the 4PPa-2PaR PM

The 4PPa-2PaR PM developed in this letter is shown in Fig. 1(a). Its moving platform is connected to the base through two legs, while each leg consists of two active joints, two proximal parallelograms, one middle link and one distal parallelogram. Each middle link is treated as a virtual passive joint that can generate 2-DOF translational motions in a vertical plane. In addition, the motion of the moving platform can be extended infinitely along its linear guide direction, and its kinematics have been analyzed in our previous work [19].

TABLE I
GEOMETRIC PARAMETERS OF THE 4PPa-2PaR PM

Symbol	Description	Unit
a	Distance between revolute joints P_1 to P_2	m
b	Distance between two linear guides	m
$\mathrm{l_u}$	Length of the proximal parallelogram	m
$\mathrm{l_d}$	Length of the distal parallelogram	m
h_1	Distance between C_j and E_j	m
h_2	Distance between F_j and P_j	m
α_j	Angle from the linear guide to $\mathrm{B}_i\mathrm{C}_j$	rad
β_j	Angle from $\mathrm{D}_j\mathrm{G}_j$ to $\mathrm{G}_j\mathrm{F}_j$	rad
φ	Acute angle from $\mathrm{D}_j\mathrm{G}_j$ to $\mathrm{D}_j\mathrm{C}_j$	rad
q_i	Displacement of prismatic joint B_i along the y-axis	m
x	x coordinate of the moving platform's center point	m
y	y coordinate of the moving platform's center point	m
z	z coordinate of the moving platform's center point	m
θ	direction angle of the x-axis of frame $\{E\}$ with respect to frame $\{B\}$	rad

Referring to Fig. 1(b), the global reference frame $\{B\}$: $O-xyz$ is fixed to linear guide I, and the local reference frame $\{E\}$: $P-x'y'z'$ is attached to the center of the moving platform. (y_1, z_1) and (y_2, z_2) represent the position coordinates of the two virtual passive joints. The pose of the moving platform is represented by four parameters, i.e., x, y, z, and θ. The geometric parameters of the 4PPa-2PaR PM are listed in Table I.

B. Kinematic Analysis

For the 4PPa-2PaR PM, its displacement kinematic relationship between the four active-joint displacements (i.e., q_1, q_2, q_3, and q_4) and the moving platform poses (i.e., x, y, z, and θ) has been derived, and the velocity Jacobian matrix, $\mathbf{G}[\dot{x} \quad \dot{y} \quad \dot{z} \quad \dot{\theta}]^T = \mathbf{J}[\dot{q}_1 \quad \dot{q}_2 \quad \dot{q}_3 \quad \dot{q}_4]^T$, has also been obtained in [19].

According to the kinematic features of the PM, the relationship between the virtual passive-joint displacements (i.e., y_1, y_2, z_1, and z_2) and the active-joint displacements (i.e., q_1, q_2, q_3, and q_4) is obtained easily as follows:

$$\begin{cases} q_1 = y_1 - \sqrt{\mathrm{l_u}^2 - z_1^2} \\ q_2 = y_1 + \sqrt{\mathrm{l_u}^2 - z_1^2} \\ q_3 = y_2 - \sqrt{\mathrm{l_u}^2 - z_2^2} \\ q_4 = y_2 + \sqrt{\mathrm{l_u}^2 - z_2^2} \end{cases}. \tag{1}$$

To determine its velocity equation, the Jacobian matrix, as the form of $\mathbf{J}_\mathrm{a}[\dot{q}_1 \quad \dot{q}_2 \quad \dot{q}_3 \quad \dot{q}_4]^T = \mathbf{J}_\mathrm{p}[\dot{y}_1 \quad \dot{y}_2 \quad \dot{z}_1 \quad \dot{z}_2]^T$ ($\mathbf{J}_\mathrm{a}$ is a identity matrix), is obtained as follows:

$$\mathbf{J}_p = \begin{bmatrix} 1 & 0 & z_1/\sqrt{\mathrm{l_u}^2 - z_1^2} & 0 \\ 1 & 0 & -z_1/\sqrt{\mathrm{l_u}^2 - z_1^2} & 0 \\ 0 & 1 & 0 & z_2/\sqrt{\mathrm{l_u}^2 - z_2^2} \\ 0 & 1 & 0 & -z_2/\sqrt{\mathrm{l_u}^2 - z_2^2} \end{bmatrix}. \tag{2}$$

Based on the (2), the determination of Jacobian matrix $\mathbf{J}_\mathrm{P}$ is derived as follows:

$$\det(\mathbf{J}_\mathrm{p}) = -4z_1 z_2 / \sqrt{\mathrm{l_u}^2 - z_1^2} \cdot \sqrt{\mathrm{l_u}^2 - z_2^2}. \tag{3}$$

When $z_1 = 0$, i.e., $q_2 - q_1 = 2\mathrm{l_u}$, the links $\mathrm{B}_1\mathrm{C}_1$ and $\mathrm{B}_2\mathrm{C}_1$ are fully stretched out. The mechanism loses a degree of freedom, and the inverse singularity occurred; when $z_1 = \mathrm{l_u}$, i.e., $q_2 = q_1$, the links $\mathrm{B}_1\mathrm{C}_1$ and $\mathrm{B}_2\mathrm{C}_1$ are fully folded back. The mechanism loses and also gains a degree of freedom, and the inverse and forward singularities occurred. The cases when $z_2 = 0$ and $z_2 = \mathrm{l_u}$ have the same singularities.

In addition, the relationship between the virtual passive-joint displacements (i.e., y_1, y_2, z_1, and z_2) and the pose parameters of the moving platform (i.e., x, y, z, and θ) is also obtained, which is given by

$$\begin{cases} x = b_1 + b_0/2 \\ y = (y_1 + y_2)/2 \\ z = z_1 + \mathrm{h}_1 - d_3 - \mathrm{h}_2 \\ \theta = \arcsin\left[(y_1 - y_2)/\mathrm{a}\right] \end{cases}, \tag{4}$$

where, $b_1 = \frac{\pm\Delta d\sqrt{-(\Delta b^2+\Delta d^2)(\Delta b^2+\Delta d^2-4\mathrm{l_d}^2)}+\Delta b\Delta d^2+\Delta b^3}{2(\Delta b^2+\Delta d^2)}$, $b_0 = \mathrm{a}\cos\theta$, $d_3 = \sqrt{\mathrm{l_d}^2 - b_1^2}$, $\Delta d = z_2 - z_1$ and $\Delta b = \mathrm{b} - b_0$.

Based on (4), the Jacobian matrix between the virtual passive joints and the moving platform, i.e., $\mathbf{J}_\mathrm{q}[\dot{y}_1 \quad \dot{y}_2 \quad \dot{z}_1 \quad \dot{z}_2]^T = \mathbf{J}_\mathrm{m}[\dot{x} \quad \dot{y} \quad \dot{z} \quad \dot{\theta}]^T$, can be obtained as follows

$$\mathbf{J}_\mathrm{q} = \begin{bmatrix} 1 & 0 & 0 & 0 \\ 0 & 1 & 0 & 0 \\ 0 & 0 & -\cos\beta_1 & 0 \\ 0 & 0 & 0 & \cos\beta_2 \end{bmatrix} \tag{5}$$

$$\mathbf{J}_\mathrm{m} = \begin{bmatrix} 0 & 1 & 0 & -(\mathrm{a}\cos\theta)/2 \\ 0 & 1 & 0 & (\mathrm{a}\cos\theta)/2 \\ \sin\beta_1 & 0 & -\cos\beta_1 & (\mathrm{a}\sin\theta\sin\beta_1)/2 \\ \sin\beta_2 & 0 & -\cos\beta_2 & -(\mathrm{a}\sin\theta\sin\beta_2)/2 \end{bmatrix} \tag{6}$$

in which, $\sin\beta_1 = x - \mathrm{a}\cos\theta/2$, $\sin\beta_2 = \mathrm{b} - x - \mathrm{a}\cos\theta/2$, $\cos\beta_1 = z_1 + \mathrm{h}_1 - z - \mathrm{h}_2$, and $\cos\beta_2 = z_2 + \mathrm{h}_1 - z - \mathrm{h}_2$. According to the (2), (5), and (6), the singularity analyses are divided into two parts by the virtual passive joints, and the simple Jacobian matrix expression forms are obtained, which is beneficial to decrease the computation burden.

C. Dynamic Modeling

The purpose of the dynamic modeling is to determine driving forces F of four active joints given the displacements, velocities and accelerations of the moving platform. Based on the geometrical characteristics of the 4PPa-2PaR PM, the Lagrangian equations are employed to formulate its dynamic model. As the displacements of active joints (i.e. q_1, q_2, q_3 and q_4) are chosen as the generalized coordinates, the Lagrangian $L(q, \dot{q})$ is formulated as

$$\mathbf{L}(\mathbf{q}, \dot{\mathbf{q}}) = \frac{1}{2}\dot{\mathbf{q}}^T\mathbf{M}(\mathbf{q})\,\dot{\mathbf{q}} - \mathbf{V}(\mathbf{q}), \tag{7}$$

in which, $\mathbf{M}(\mathbf{q})$ is the manipulator inertia matrix and $\mathbf{V}(\mathbf{q})$ is the potential energy. To obtain the joint-space inertia matrix, the Jacobian matrices of proximal link $\mathrm{B}_i\mathrm{C}_j$ $(i = 1, 2, j = 1; i = 3, 4, j = 2)$ and distal link $\mathrm{E}_j\mathrm{H}_j$ $(j = 1, 2)$ are necessary to be analyzed.

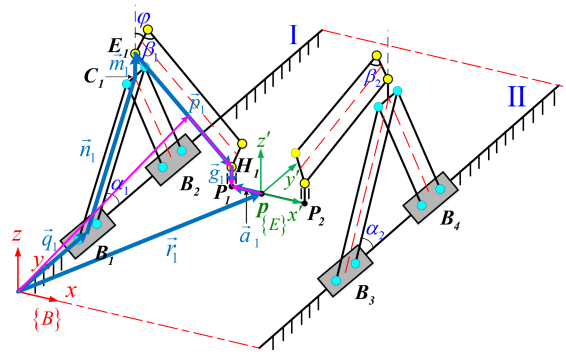

Fig. 2. Two closed-loop vectors from the base coordinate origin to the center of the moving platform and the distal link $\mathrm{E}_1\mathrm{H}_1$.

1) Angular Velocity Analysis of Links BC *and* EH*:* According to the geometrical relationship between proximal link $\mathrm{B}_i\mathrm{C}_j$ and four active joints, the angular velocities $\dot{\alpha}_1$ and $\dot{\alpha}_2$ are derived readily as follows

$$\begin{cases} \dot{\alpha}_1 = (\dot{q}_1 - \dot{q}_2)/2\mathrm{l_u}\sin\alpha_1, \\ \dot{\alpha}_2 = (\dot{q}_3 - \dot{q}_4)/2\mathrm{l_u}\sin\alpha_2. \end{cases} \tag{8}$$

To determine the angular velocities $\dot{\beta}_1$ and $\dot{\beta}_2$ of distal link E_jH_j, a closed-loop vector approach is employed, as shown in Fig. 2. Let the closed-loop vector from the origin of frame $\{B\}$ to frame $\{E\}$ be $\mathbf{r}_i = [x \quad y \quad z\ ]^{\mathrm{T}} (i = 1, 2, 3, 4)$, it yields

$$\begin{cases} \mathbf{r}_i = \mathbf{q}_i + \mathrm{l_u}\mathbf{n}_i + \mathrm{h_1}\mathbf{m}_i + \mathrm{l_d}\mathbf{p}_i + \mathrm{h_1}\mathbf{m}_i - \frac{\mathrm{a}}{2}\mathbf{a}_j \\ (i = 1, 2; j = 1), \\ \mathbf{r}_i = \mathbf{b} + \mathbf{q}_i + \mathrm{l_u}\mathbf{n}_i + \mathrm{h_1}\mathbf{m}_i + \mathrm{l_d}\mathbf{p}_i + \mathrm{h_1}\mathbf{g}_i - \frac{\mathrm{a}}{2}\mathbf{a}_j \\ (i = 3, 4; j = 2), \end{cases} \tag{9}$$

where, $\mathbf{q}_i$ is the displacement of active joints; $\mathbf{b}$ represents the distance between two linear guides along x-axis; $\mathbf{n}_i$, $\mathbf{m}_i$, $\mathbf{p}_i$, and $\mathbf{g}_i$ represent the unit direction vectors of $\overrightarrow{\mathrm{B}_i\mathrm{C}_j}$, $\overrightarrow{\mathrm{C}_j\mathrm{E}_j}$, $\overrightarrow{\mathrm{E}_j\mathrm{H}_j}$, and $\overrightarrow{\mathrm{H}_j\mathrm{P}_j}$, respectively; $\mathbf{a}_j$ is a vector from the origin of frame $\{E\}$ to the points P_j. The velocity equation is obtained by taking the derivative of (9) with respect to time, which is given by

$$\dot{\mathbf{r}}_i = \mathbf{K}_{qi}\dot{\mathrm{q}}_i + \mathbf{K}_{ui}\mathrm{l_u}\dot{\alpha}_i + \mathbf{K}_{di}\mathrm{l_d}\dot{\beta}_i - \mathbf{K}_{ai}\dot{\theta}_i \tag{10}$$

in which, $\mathbf{K}_{qi}$, $\mathbf{K}_{ui}$, $\mathbf{K}_{di}$, and $\mathbf{K}_{ai} \in \mathbb{R}^{3\times1}$ are all coefficient vectors.

Substituting (8) into (10), the angular velocity $\dot{\beta}_j$ is given by

$$\begin{cases} \dot{\beta}_1 = \dot{x}/(\mathrm{l_d}\cos\beta_1) + (\mathrm{a}\sin\theta)\dot{\theta}/(2\mathrm{l_d}\cos\beta_1), \\ \dot{\beta}_2 = -\dot{x}/(\mathrm{l_d}\cos\beta_2) + (\mathrm{a}\sin\theta)\dot{\theta}/(2\mathrm{l_d}\cos\beta_2). \end{cases} \tag{11}$$

2) Jacobian Matrices of Links BC and EH: For the link $\mathrm{B}_i\mathrm{C}_j$, its coordinate of center point (i.e. $x_{\mathrm{lu}i}$, $y_{\mathrm{lu}i}$, and $z_{\mathrm{lu}i}$) can be described by q_i. By taking the derivative of the displacement equations, the velocity of link $\mathrm{B}_1\mathrm{C}_1$ can be determined by the form of $[\dot{x}_{\mathrm{lu_1}} \quad \dot{y}_{\mathrm{lu_1}} \quad \dot{z}_{\mathrm{lu_1}} \quad \dot{\alpha}_1]^T = \mathbf{J}_{\mathrm{lu_1}}[\dot{q}_1 \quad \dot{q}_2 \quad \dot{q}_3 \quad \dot{q}_4]^T$. which can be given by

$$\mathbf{J}_{\mathrm{lu_1}} = \begin{bmatrix} 0 & 0 & 0 & 0 \\ 3/4 & 1/4 & 0 & 0 \\ 1/4 & -1/4 & 0 & 0 \\ 1/(2lu\sin\alpha_1) & -1/(2lu\sin\alpha_1) & 0 & 0 \end{bmatrix}, \tag{12}$$

Similarly, the Jacobian matrices of links $\mathrm{B}_2\mathrm{C}_1$, $\mathrm{B}_3\mathrm{C}_2$, and $\mathrm{B}_4\mathrm{C}_2$ can also be derived.

To obtain the Jacobian matrix of distal link $\mathrm{E}_j\mathrm{H}_j$ $(j = 1, 2)$, a closed-loop vector form the origin of frame $\{B\}$ to the center point of distal links $\mathrm{E}_j\mathrm{H}_j$ is employed, as shown in Fig. 2. Hence, The velocity equation of link $\mathrm{E}_1\mathrm{H}_1$ is calculated as follows

$$\begin{bmatrix} \dot{x}_{\mathrm{ld_1}} & \dot{y}_{\mathrm{ld_1}} & \dot{z}_{\mathrm{ld_1}} \end{bmatrix}^{\mathrm{T}} = \begin{bmatrix} \dot{x} & \dot{y} & \dot{z} \end{bmatrix}^{\mathrm{T}} + \mathbf{K}_{\mathrm{a}}\dot{\theta} + \mathbf{K}_{\mathrm{d}}\dot{\beta}_1, \tag{13}$$

in which, $\mathbf{K}_{\mathrm{a}} = \frac{a}{2}[\sin\theta \quad -\cos\theta \quad 0\ ]^T$ and $\mathbf{K}_{\mathrm{d}} = \frac{\mathrm{l_d}}{2}[-\cos\beta_1 \quad 0 \quad -\sin\beta_1\ ]^T$. Substituting (11) into (13), the velocity equation can be represented as the form of $[\dot{x}_{\mathrm{ld1}} \quad \dot{y}_{\mathrm{ld1}} \quad \dot{z}_{\mathrm{ld1}} \quad \dot{\beta}_1\ ]^T = \mathbf{J}_{\beta_1}[\dot{x} \quad \dot{y} \quad \dot{z} \quad \dot{\theta}\ ]^T$, and the Jacobian matrix $\mathbf{J}_{\beta_1}$ is given by

$$\mathbf{J}_{\beta_1} = \begin{bmatrix} 1/2 & 0 & 0 & \mathrm{a}\sin\theta/4 \\ 0 & 1 & 0 & -\mathrm{a}\cos\theta/2 \\ -\tan\beta_1/2 & 0 & 1 & -\mathrm{a}\sin\theta\tan\beta_1/4 \\ 1/(\mathrm{l_d}\cos\beta_1) & 0 & 0 & \mathrm{a}\sin\theta/(2\mathrm{l_d}\cos\beta_1) \end{bmatrix}. \tag{14}$$

Based on the velocity relationship between the moving platform and active joints, i.e., $[\dot{x} \quad \dot{y} \quad \dot{z} \quad \dot{\theta}\ ]^{\mathrm{T}} = \mathbf{J}_p[\dot{q}_1 \quad \dot{q}_2 \quad \dot{q}_3 \quad \dot{q}_4\ ]^{\mathrm{T}}$, the velocity equation of link $\mathrm{E}_1\mathrm{H}_1$ is rewritten as

$$\begin{bmatrix} \dot{x}_{\mathrm{ld_1}} & \dot{y}_{\mathrm{ld_1}} & \dot{z}_{\mathrm{ld_1}} & \dot{\beta}_1 \end{bmatrix}^{\mathrm{T}} = \mathbf{J}_{\mathrm{ld_1}}\begin{bmatrix} \dot{q}_1 & \dot{q}_2 & \dot{q}_3 & \dot{q}_4 \end{bmatrix}^{\mathrm{T}}. \tag{15}$$

where, $\mathbf{J}_{\mathrm{ld_1}} = \mathbf{J}_{\beta_1}\mathbf{J}_p$. Similarly, the Jacobian matrix of distal link $\mathrm{E}_2\mathrm{H}_2$ can be represented as $\mathbf{J}_{\mathrm{ld_2}} = \mathbf{J}_{\beta_2}\mathbf{J}_p$.

3) Dynamic Equations: The generalized force is represented explicitly as

$$F_i = \sum_{j=1}^{n}\mathbf{M}_{ij}(\mathbf{q})\ddot{q}_j + \sum_{j,k=1}^{n}\mathbf{\Gamma}_{ijk}\dot{q}_j\dot{q}_k + N_i(\mathbf{q}), \tag{16}$$

where $\mathbf{\Gamma}_{ijk} = \frac{1}{2}(\frac{\partial\mathbf{M}_{ij}(\mathbf{q})}{\partial q_k} + \frac{\partial\mathbf{M}_{ik}(\mathbf{q})}{\partial q_j} + \frac{\partial\mathbf{M}_{kj}(\mathbf{q})}{\partial q_i})$. In addition, $\mathbf{M}(\mathbf{q})$ and $\mathbf{N}(\mathbf{q})$ can be derived as respectively

$$\begin{cases} \mathbf{M}(\mathbf{q}) = \mathbf{J}_{\mathrm{l_u}}^{\mathrm{T}}\boldsymbol{\mathcal{M}}_{\mathrm{l_u}}\mathbf{J}_{\mathrm{l_u}} + \mathbf{J}_{\mathrm{l_d}}^{\mathrm{T}}\boldsymbol{\mathcal{M}}_{\mathrm{l_u}}\mathbf{J}_{\mathrm{l_d}} + \mathbf{J}_{\mathrm{p}}^{\mathrm{T}}\boldsymbol{\mathcal{M}}_{\mathrm{p}}\mathbf{J}_{\mathbf{p}}, \\ \mathbf{N}(\mathbf{q}) = \partial V_{\mathrm{l_u}}/\partial\mathbf{q} + \partial V_{\mathrm{l_d}}/\partial\mathbf{q} + \partial V_{\mathrm{P}}/\partial\mathbf{q}, \end{cases} \tag{17}$$

in which, $\boldsymbol{\mathcal{M}}_{\mathrm{l_u}}$, $\boldsymbol{\mathcal{M}}_{\mathrm{l_d}}$, and $\boldsymbol{\mathcal{M}}_{\mathrm{p}}$ are 4×4 inertia matrices; $\mathbf{J}_{\mathrm{l_u}}$, $\mathbf{J}_{\mathrm{l_d}}$ and $\mathbf{J}_{\mathrm{p}}$ are Jacobian matrices; $V_{\mathrm{l_u}}$, $V_{\mathrm{l_d}}$, and V_{p} are potential energies of links $\mathrm{B}_i\mathrm{C}_j$, $\mathrm{E}_j\mathrm{H}_j$ $(i = 1, 2, j = 1; i = 3, 4, j = 2)$, and the moving platform respectively, which are given by

$$\begin{cases} V_{\mathrm{l_u}} = \frac{1}{2}\mathrm{m_{l_u}}\mathrm{g}\mathrm{l_u}\sin\alpha_j, \\ V_{\mathrm{l_d}} = \frac{1}{2}\mathrm{m_{l_d}}\mathrm{g}(2\mathrm{h_1} - \mathrm{l_d}\cos(\beta_j - \varphi) + 2\mathrm{l_u}\sin\alpha_j), \\ V_p = \frac{1}{2}\mathrm{m_p}\mathrm{g}(2\mathrm{h_1} - \mathrm{l_d}\cos(\beta_1 - \varphi) - \mathrm{l_d}\cos(\beta_2 - \varphi) \\ \qquad +\mathrm{l_u}\sin\alpha_1 + \mathrm{l_u}\sin\alpha_2 - 2\mathrm{h_2}), \end{cases} \tag{18}$$

Substituting (17) and (18) into (16), the dynamic equation is formulated as the form of

$$\mathbf{F} = \mathbf{M}(\mathbf{q})\ddot{\mathbf{q}} + \mathbf{C}(\mathbf{q}, \dot{\mathbf{q}})\dot{\mathbf{q}} + \mathbf{N}(\mathbf{q},). \tag{19}$$

To validate the correctness of the dynamic model, a simulation example is given in MATLAB and ADAMS environments by $q_1 = q_3 = 0.18{+}0.1\sin\mathrm{t}$ and $q_2 = q_4 = 0.90{+}0.1\sin\mathrm{t}$, and the simulation results are shown in Fig. 3.

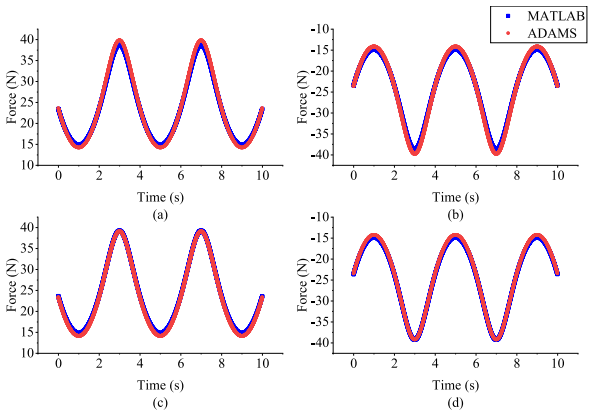

Fig. 3. Simulation results in MATLAB and ADAMS environments: (a) driving force of active joint 1; (b) driving force of active joint 2; (c) driving force of active joint 3; (d) driving force of active joint 4.

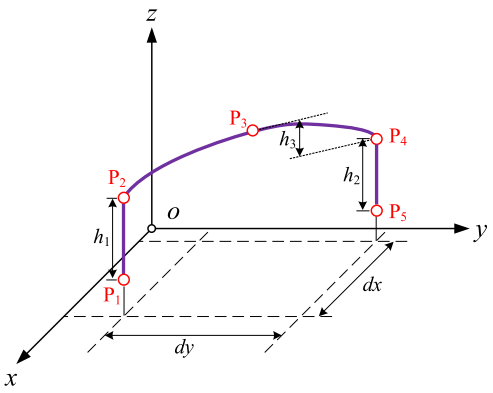

Fig. 4. Geometric path of pick-and-place operation in base frame.

III. Trajectory Generation in the Virtual Passive-Joint Space Based on Quintic B-Splines

A. Description of the Geometric Path

To describe the geometric path of pick-and-place operations in Cartesian space, a common method is employed through given five via points. As shown in Fig. 4, $\mathrm{P}_1(x_1, y_1, z_1, \theta_1)$, $\mathrm{P}_2(x_2, y_2, z_2, \theta_2)$, $\mathrm{P}_3(x_3, y_3, z_3, \theta_3)$, $\mathrm{P}_4(x_4, y_4, z_4, \theta_4)$ and $\mathrm{P}_5(x_5, y_5, z_5, \theta_5)$ are the initial point, lift-off point, middle point, set-down point, and final point, respectively. h_1 and h_2 represent the heights of $\| \mathrm{P}_1\mathrm{P}_2 \|$ and $\| \mathrm{P}_4\mathrm{P}_5 \|$ segments, and h_3 is the height difference between P_3 and P_2 (P_4) along z-axis direction in base frame. In addition, the distances between P_1 and P_5 are represented by d_x and d_y in x- and y-axis directions, respectively.

B. Generation of the Trajectory Model by Quintic B-Splines

A brief review of quintic B-splines is displayed as follows. A B-spline of degree 5, i.e., $k = 5$, is a linear combination of Bernstein basic function $N_{i,k}(u)$, which is weighted by control points Q_i. The motion profile $s(u)$ is formulated as

$$s(u) = \sum_{i=1}^{n} Q_i \cdot N_{i,k}(u), 0 \le u \le 1, \tag{20}$$

in which, $N_{i,k}(u)$ can be obtained by the De-Boor formulations. Let t_i ($i = 1, \ldots, v$-1) denotes the execution time of each trajectory segments divided by the via points (v is the number of the via points), and $t_{all} = \sum_{i=1}^{v-1} t_i$. u_i can be derived by the cumulative chord length approach as follows:

$$u_i = \begin{cases} 0, 1 \le i \le k+1 \\ u_{i-1} + \frac{t_{i-k-2}}{t_{all}}, k+2 \le i \le k+v+1 \\ 1, k+v+2 \le i \le 2\tilde{}k+v+2. \end{cases} \tag{21}$$

To achieve the jerk continuity, two virtual points are introduced at u_{k+2} and u_{k+v+2} positions, and the node u_i is repeated 6 times at $u_i = 0$ and $u_i = 1$ positions. The number of v constraint equations is formulated as follows

$$\begin{cases} s(u_{k+1}) = Q_1 \\ s(u_{k+j}) = \sum_{i=1}^{n} Q_i \cdot N_{i,k}(u_{k+j}), j = 2, 3, v-1. \\ s(u_{k+v+2}) = Q_n \end{cases} \tag{22}$$

According to the r-th (r=1,2,3) derivative form of $s(u)$ with respect to u, 6 constraint equations are used to satisfy boundary conditions in terms of velocity, acceleration and jerk at both ends of the trajectory, they are given by

$$\begin{cases} Q_{1,r}(u_1) = \sum_{i=1}^{r+1} Q_{i,r} \cdot C_{i,r} = 0 \\ Q_{n-1,r}(u_{k+v+2}) = \sum_{i=n-r}^{n} Q_{i,r} \cdot C_{i,r} = 0 \end{cases} r = 1, 2, 3, \tag{23}$$

in which, $C_{i,r}$ can be determined by the derivative form of $s(u)$. The coordinates of the control points can be rewritten in a matrix form as follows

$$\mathbf{Q} = \mathbf{A}^{-1}\mathbf{B}, \tag{24}$$

where $\mathbf{Q} = [Q_1 \cdots Q_n \ ]^T_{1\times n}$, $\mathbf{A} = [\mathbf{A}_1 \mathbf{A}_2 \ ]^T$, $\mathbf{B} = [\mathbf{B}_1 \mathbf{B}_2 \ ]^T$, $\mathbf{B}_1 = [s_1 \cdots s_v \ ]^T_{1\times v}$, $\mathbf{B}_2 = [0 \cdots 0 \ ]^T_{1\times 6}$, while $[\mathbf{A}_1]_{v\times n}$ and $[\mathbf{A}_2]_{6\times n}$ can be obtained according to (23).

IV. Time-Optimal Trajectory Planning in the Virtual Passive-Joint Space

A. Formulation of the Optimization Model

In general, a trajectory that can achieve pick-and-place operation in minimum time is expected. For the 4PPa-2PaR PM, a time-optimal trajectory planning model in the virtual passive-joint space with design parameters and constraint conditions is formulated as follows:

$$\min_{t_i} \ t_{all} = t_1 + t_2 + t_3 + t_4 \ (i = 1, \ldots, 4)$$

$$s.t.$$

$$0 < t_i < 2\,\mathrm{s}, \tag{a}$$

$$0 < q_2 - q_1 < 2l_u, \tag{b}$$

$$0 < q_4 - q_3 < 2l_u, \tag{c}$$

$$|(q_2 + q_1)/2 - (q_4 + q_3)/2| < a, \tag{d}$$

$$\dot{q}_i \leq 2\,\mathrm{m/s}, \tag{e}$$

$$F_i \leq 100\,\mathrm{N}, \tag{f}$$

$$\max\left(J_x, J_y, J_z\right) \leq 35\,\mathrm{m/s^3}, \tag{g}$$

in which, t_i is the design parameter, and t_{all} is the objective function. q_i and $\dot{q}_i$ represent the displacement and velocity of the active joints; F_i is the driving force; J_x, J_y, and J_z are the translational jerks of the moving platform, respectively. (a) is a boundary constraint for each of trajectory segments, and (b) to (d) are given to satisfy the trajectory without suffering from the kinematics singularity and the mechanical interference; (e) and (f) are velocity of the active joints and the driving forces constraint conditions; (g) is a translational jerk constraint for the trajectory smoothness of the moving platform.

B. Optimization Algorithm

As the objective function has a highly nonlinear relationship with constrain conditions, *Genetic Algorithm* (GA) is employed to formulate the optimization model in MATLAB environment. GA is a global search method to solve optimization problems, and its process is affected mainly by three parameters, i.e., the population size, the crossover operator, and the mutation operator. Based on the nonlinear and constraint optimization problems, their general boundary conditions are 20–100, 0.4–0.9, and 0.001–0.1, respectively. To obtain the appropriate values for these parameters, a large number of simulations have been conducted. According to the results, the three optimal values are 50, 0.8 and 0.01, respectively.

V. Simulation Results

To validate the effectiveness of the virtual passive-joint space method, a simulation example is given by practical requirements. The main purpose of the simulation example is to obtain the minimum trajectory time. Besides, other trajectory performances, i.e., the driving forces of four active joints, the jerk values of the moving platform, the accuracy of the geometric path, and the computational efficiency, are also validated, respectively.

Based on the pick-and-place operation requirements, a set of path parameters is given in Cartesian space, i.e., $h_1 = h_2 = 0.1\,\mathrm{m}$, $h_3 = 0.05\,\mathrm{m}$, $d_x = 0.2\,\mathrm{m}$, d_y=0.5 m, $\theta_1 = \theta_2 = 0$, $\theta_4 = \theta_5 = \pi/3$, and $\theta_3 = (\theta_1 + \theta_5)/2$. Hence, the coordinates of the moving platform are $P_1(0.3, 1, -0.2, 0)$, $P_2(0.3, 1, -0.1, 0)$, $P_3(0.4, 0.75, -0.05, \pi/6)$, $P_4(0.5, 0.5, -0.1, \pi/3)$ and $P_5(0.5, 0.5, -0.2, \pi/3)$, respectively. According to the inverse kinematics, the coordinates of the virtual passive joints $(y_{1i}, y_{2i}, z_{1i}, z_{2i})$ $(i = 1, 2, \ldots, 5)$ can be derived.

A. Minimum Time

Based on the time-optimal trajectory planning model in the virtual passive-joint space, the minimum execution time for the pick-and-place operation is obtained, as shown in Fig. 5. According to the simulation result, the objective function begins to converge stably after the 20 th generation, and the best fitness value is 2.05 s. The comparison of the optimized objective function and the design parameters produced by three different methods are shown in Table II.

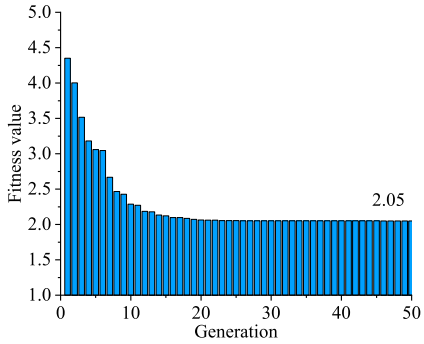

Fig. 5. Curves of the best fitness value with evolutionary generations.

TABLE II
Simulation Results of Objective Functions and Design Parameters With Three Different Trajectory Planning Methods

	Function	Design parameters			
Methods	$t_{all}(s)$	$t_1(s)$	$t_2(s)$	$t_3(s)$	$t_4(s)$
A-method	2.11	0.28	0.29	0.46	1.08
P-method	2.05	0.33	0.27	0.44	1.02
C-method	2.23	0.40	0.28	0.41	1.14

The simulation results show that the optimal-time trajectory with multiple constraints generated in the virtual passive-joint space is the fastest among the three methods. The trajectory planned in active-joint space is limited by the jerk constraint mainly, which takes more time to satisfy the jerk constraint. In addition, the velocity and driving forces constraints prolong the trajectory time planned in Cartesian space due to the high kinematic nonlinearity. The kinematic mappings from the virtual passive-joint space to both the active-joint space and Cartesian space have a low degree of nonlinearity because of the decomposed kinematic models, so the virtual passive-joint space method generates the fastest trajectory.

B. Driving Forces of the Active Joints

Based on three optimization results, the driving force curves of active joints are derived by the dynamic model, as shown in Fig. 6. In general, the average and peak values are employed to evaluate the performances of driving forces. The average values generated in virtual passive-joint space are close to those of the active-joint space method and Cartesian space method, and they are decreased slightly by 0.56% and 2.1%, respectively.

Although the driving force curves generated by three method have similar tendency, the peak driving forces have different values. Fig. 6(a) and (d) show that the peak values of the active joints B_1 and B_4 are decreased by 15.9% and 13.4% compared with that of the active-joint space method, and only decreased by 2.5% and 6.0% compared with that of Cartesian space method, while Fig. 6(b) and (c) indicate that three peak driving forces of the active joints B_2 and B_3 have the nearly same values.

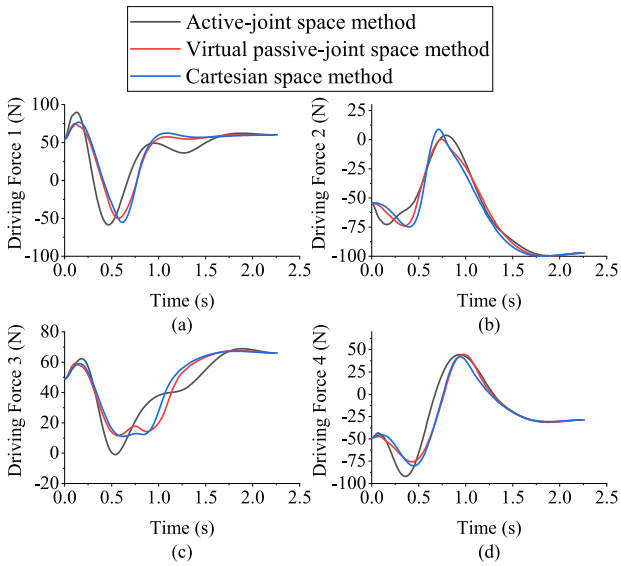

Fig. 6. Driving force curves of active joints: (a) driving force of B_1; (b) driving force of B_2; (c) driving force of B_3; (d) driving force of B_4.

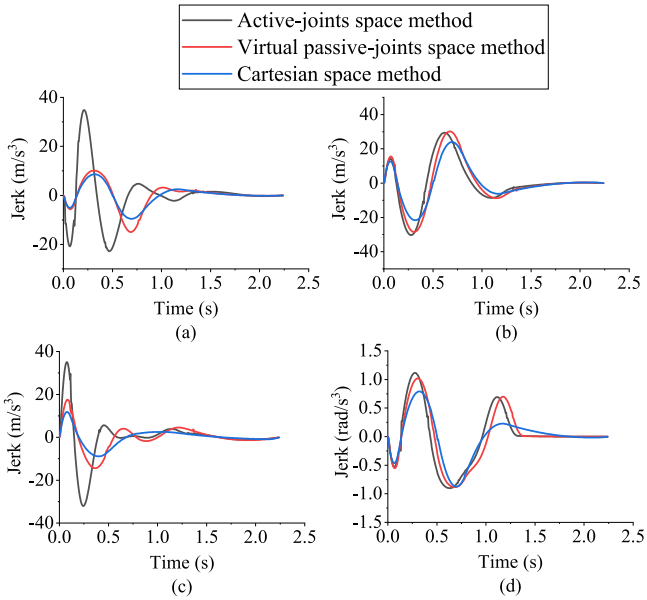

Fig. 7. Jerk curves of the moving platform: (a) x-direction; (b) y-direction; (c) z-direction; (d) θ-direction.

C. Jerk Values of the Moving Platform

According to the optimized design parameters, the displacements, velocities, accelerations, and jerks of the moving platform are all derived. As shown in Fig. 7, three jerk curves of the moving platform are generated in the active-joint space, the virtual passive-joint space and Cartesian space, respectively. The virtual passive-joint space method decreases its average and peak values of jerk by 14.6% and 37.6% compared with the active-joint space method, especially they are decreased by 37.8% and 53.7% along the x-axis direction, and decreased by 21.9% and 51.4% along the z-axis direction. In addition, the

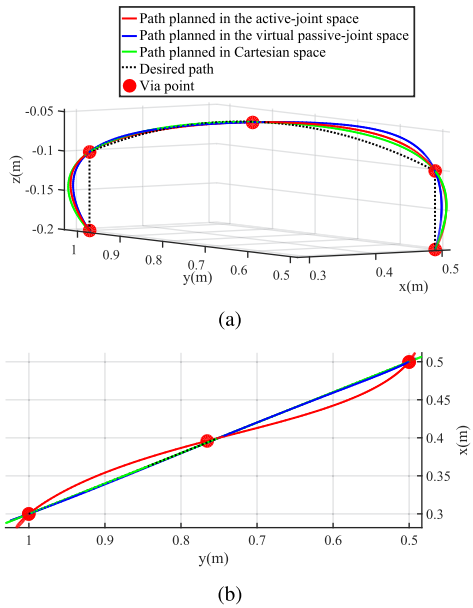

Fig. 8. Three different geometric paths of the moving platform: (a) front view; (b) top view.

average and peak values of the trajectory planned in virtual passive-joint space are increased by 27.66% and 37.3% compared with the results of Cartesian space method.

D. Path Accuracy and Computational Efficiency

For the high-speed pick-and-place operation, the path accuracy of the moving platform is also a vital index. Based on the optimized results, three different geometric paths are obtained as shown in Fig. 8. Owing to the high nonlinear kinematic mapping from the active joints to the moving platform, the path generated by active-joint space method deviates from the desired path plane, especially in the x-axis and y-axis directions, while the paths generated in virtual passive-joint space and Cartesian space coincide with the desired trajectory plane due to the low degree of nonlinear kinematic mappings. Based on the distance of the trajectory deviating from the ideal path plane, the path generated in virtual passive-joint space is more accurate than that in the active-joint space.

In addition, the computation time are validated by running the MATLAB program code. With the computer configuration of Legion R7000P and AMD Ryzen 7 4800H, 20 groups of simulation tests are conducted. The results show that the average running time are 1.95 s, 2.09 s, and 2.38 s in the active-joint space, the virtual passive-joint space and Cartesian space, respectively. Compared with Cartesian space method, the computation efficiency is improved by 12.2%, which indicates the effectiveness of the virtual passive-joint space method.

E. Performance Comparisons of the Three Trajectories

To justify the advantages of the virtual passive-joint space method clearly, three trajectories are compared in terms of

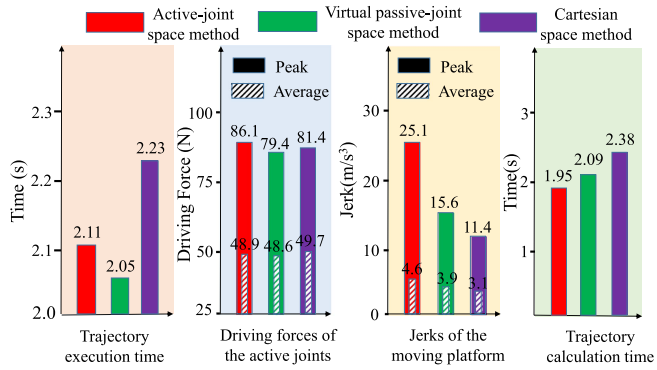

Fig. 9. Comparisons of trajectory performances generated by three different methods.

TABLE III
COMPARISONS OF MULTIPLE DIFFERENT TRAJECTORY EXAMPLES

Example1	Time(s)	Force(N)		Jerk(N/m^3)	
Methods	t_{all}	Peak	Average	Peak	Average
A-method	1.67	87.8	54.3	28.3	8.9
P-method	1.53	89.4	57.4	26.6	8.0
C-method	1.61	93.5	58.1	19.6	7.8

Example2	Time(s)	Force(N)		Jerk(N/m^3)	
Methods	t_{all}	Peak	Average	Peak	Average
A-method	1.98	84.7	52.7	25.0	7.6
P-method	1.92	78.1	49.4	22.2	6.2
C-method	2.16	77.6	53.6	13.3	4.5

Example3	Time(s)	Force(N)		Jerk(N/m^3)	
Methods	t_{all}	Peak	Average	Peak	Average
A-method	1.87	98.8	51.2	23.9	7.2
P-method	1.84	88.7	49.2	14.2	6.1
C-method	1.92	90.7	49.6	11.4	3.1

trajectory execution time, driving forces, jerk of the moving platform, and trajectory calculation time (the comparison of the path accuracy is shown in Fig. 8), as shown in Fig. 9. In addition, multiple different trajectories with the same constraints are given to validate the effectiveness of the virtual passive-joint space method, the comparisons are presented in Table III.

VI. CONCLUSION

For the 4-DOF (3T1R) 4PPa-2PaR PM with a unique four-to-two leg structure, a trajectory planning method in the two 2-DOF virtual passive-joint spaces is proposed in this letter. Compared with the conventional trajectory planning methods in either active-joint space or Cartesian space, the new method simplifies the kinematics analysis and decreases the kinematics nonlinearity, so the overall performance is improved. For the trajectory planning in the virtual passive-joint space, the displacement and velocity kinematics between passive joints and both the active joints and the moving platform are analyzed. The closed-loop dynamic model is formulated by utilizing the Lagrangian method, and the quintic B-spline is employed to generate the trajectories. An optimization model is formulated by GA to search the time-optimal trajectory. The simulation results show that the motion time planned in the virtual passive-joint space is decreased by 2.8% and 8.1% compared with the active-joint space method and Cartesian space method respectively. The average and peak jerks of the moving platform are decreased by 14.6% and 37.6% compared with the active-joint space method. Besides, the comparisons of driving forces, geometric path, and computation burden are all provided to verify the effectiveness of the virtual passive-joint space method. Future work will be focused on the experimental verification of the proposed trajectory planing method on prototype of the 4PPa-2PaR PM.

REFERENCES

[1] W. D. Zhu, B. Zi, K. Bao, and S. Qian, "Dynamic trajectory planning for a three degrees-of-freedom cable-driven parallel robot using quintic B-splines," *J. Mech. Des.*, vol. 142, no. 7, 2020, Art. no. 073301.
[2] H. Wang, H. Wang, J. Huang, B. Zhao, and L. Quan, "Smooth point-to-point trajectory planning for industrial robots with kinematical constraints based on high-order polynomial curve," *Mechanism Mach. Theory*, vol. 139, pp. 284–293, 2019.
[3] M. Farajtabar, H. M. Daniali, and S. M. Varedi, "Pick and place trajectory planning of planar 3-RRR parallel manipulator in the presence of joint clearance," *Robotica*, vol. 35, no. 2, pp. 241–253, 2015.
[4] J. Jahanpour, M. Motallebi, and M. Porghoveh, "A novel trajectory planning scheme for parallel machining robots enhanced with NURBS curves," *J. Intell. Robotic Syst.*, vol. 82, pp. 257–275, 2016.
[5] C. D. Porawagama and S. R. Munasinghe, "Reduced jerk joint space trajectory planning method using 5-3-5 spline for robot manipulators," in *Proc. IEEE 7th Int. Conf. Inf. Automat. Sustain.*, 2014, pp. 1–6.
[6] Z. Xie, F. Xie, X.-J. Liu, and J. Wang, "Global G3 continuity toolpath smoothing for a 5-DoF machining robot with parallel kinematics," *Robot. Comput.- Integr. Manuf.*, vol. 67, 2021, Art. no. 102018.
[7] B. Su and L. Zou, "Manipulator trajectory planning based on the algebraic-trigonometric hermite blended interpolation spline," *Procedia Eng.*, vol. 29, pp. 2093–2097, 2012.
[8] U. Dinçer and M. Çevik, "Improved trajectory planning of an industrial parallel mechanism by a composite polynomial consisting of Bézier curves and cubic polynomials," *Mechanism Mach. Theory*, vol. 132, pp. 248–263, 2019.
[9] R. J. Moreno Masey, J. O. Gray, T. J. Dodd, and D. G. Caldwell, "Elliptical point to point trajectory planning using electronic cam motion profiles for high speed industrial pick and place robots," in *Proc. IEEE Conf. Emerg. Technol. Factory Automat.*, 2009, pp. 1–8.
[10] X. Zhang and Z. Ming, "Trajectory planning and optimization for a Par4 parallel robot based on energy consumption," *Appl. Sci.*, vol. 9, no. 13, 2019, Art. no. 2770.
[11] T. Su, L. Cheng, Y. Wang, X. Liang, J. Zheng, and H. Zhang, "Time-optimal trajectory planning for delta robot based on quintic Pythagorean-Hodograph curves," *IEEE Access*, vol. 6, pp. 28530–28539, 2018.
[12] D. Yang, F. Xie, and X. Liu, "Velocity constraints based online trajectory planning for high-speed parallel robots," *Chin. J. Mech. Eng.*, vol. 35, no. 1, pp. 1–12, 2022.
[13] P. Huang, Y. Xu, and B. Liang, "Tracking trajectory planning of space manipulator for capturing operation," *Int. J. Adv. Robot. Syst.*, vol. 3, no. 3, pp. 1014–1019, 2008.
[14] Y. Li, T. Huang, and D. G. Chetwynd, "An approach for smooth trajectory planning of high-speed pick-and-place parallel robots using quintic B-splines," *Mechanism Mach. Theory*, vol. 126, pp. 479–490, 2018.
[15] R. Xu, J. Tian, X. Zhai, J. Li, and J. Zou, "Research on improved hybrid polynomial interpolation algorithm for rail inspection robot," in *Proc. 5th Int. Conf. Electron. Inf. Technol. Comput. Eng.*, 2021, pp. 1207–1213.
[16] S. Hu, H. Kang, H. Tang, Z. Cui, Z. Liu, and P. Ouyang, "Trajectory optimization algorithm for a 4-DOF redundant parallel robot based on 12-phase sine jerk motion profile," *Actuators*, vol. 10, no. 4, 2021, Art. no. 80.
[17] M. R. Azizi and R. Khani, "An algorithm for smooth trajectory planning optimization of isotropic translational parallel manipulators," *Proc. Inst. Mech. Eng., Part C: J. Mech. Eng. Sci.*, vol. 230, no. 12, pp. 1987–2002, 2015.
[18] G. Yang, I.-M. Chen, W. Lin, and J. Angeles, "Singularity analysis of three-legged parallel robots based on passive-joint velocities," *IEEE Trans. Robot. Automat.*, vol. 17, no. 4, pp. 413–422, Aug. 2001.
[19] J. Zhao et al., "Kinematics analysis and workspace optimization for a 4-DOF 3T1R parallel manipulator," *Mechanism Mach. Theory*, vol. 167, 2022, Art. no. 104484.